IEEE Access
Multidisciplinary ⋮ Rapid Review ⋮ Open Access Journal

Received January 6, 2020, accepted January 13, 2020, date of publication January 15, 2020, date of current version January 24, 2020.

Digital Object Identifier 10.1109/ACCESS.2020.2966922

Reliability Modeling of PV Systems Based on Time-Varying Failure Rates

HAMZA ABUNIMA AND JIASHEN TEH, (Member, IEEE)
School of Electrical and Electronic Engineering, Engineering Campus, Universiti Sains Malaysia, Penang 14300, Malaysia

Corresponding author: Jiashen Teh (jiashenteh@usm.my)

This work was supported in part by the Universiti Sains Malaysia (USM) Research University Incentive (RUI) under Grant 1001/PELECT/8014099, and in part by the Ministry of Education Malaysia Fundamental Research Grant Scheme (FRGS) under Grant 203/PELECT/6071442.

ABSTRACT The penetration of photovoltaic (PV) systems in power grids has substantially increased since the recognition of renewable energies. In a high solar-integrated network environment, an accurate forecast of the expected solar energy output is vital. One of the important factors that influence such forecast is the failure rates of PV systems. Therefore, a new and realistic reliability model of the PV system is proposed in this study. In contrast to the conventional reliability model, which uses fixed values of failure rates in a year, the proposed model considers various weather conditions, detailed PV system architecture, manufacturing quality and other necessary materials to determine the time-varying failure rates of the PV system. Results reveal that the proposed model produces monthly failure rates that are considerably different from the fixed yearly failure rate in which the difference in high latitude regions is more significant than that in tropical climate regions.

INDEX TERMS Failure rate, PV system, reliability, time-varying.

I. INTRODUCTION

Increasing concerns regarding global warming and dwindling fossil fuels have led to the development of renewable energy (RE) systems. Amongst various RE sources, solar energy is one of the most promising due to its large untapped natural capacity for power generation. In 2018, the earth received approximately 1.2×10^{17}kWh of solar energy, but the estimated energy consumption in the same year was only 1.6×10^{11} kWh [1]. This finding indicates that solar energy matches the load demands by approximately 12,500 times on a per-minute basis. Solar energy usage in domestic and industrial power supplies has dramatically increased by seventy-fold from 2007 to 2017, subsequently reducing the costs of solar energy worldwide [2]. In the next two decades, the share of photovoltaic (PV) systems is expected to increase further, constituting 23% of the total global power generation; such increase is mostly due to large-scale, grid-connected PV farms, which cause significant changes in existing generation systems [3]. Therefore, understanding the reliability of the PV system and providing accurate quantification are crucial [4], [5].

The initial reliability modelling of PV systems neglects the partial failures of the individual components [6], [7]. The components of the PV system, such as panels, converters, inverters, fuses and connectors, respond differently to various environmental conditions [8]–[11]. Thus, weather and ageing records have been used to determine the time-varying failure rates of PV systems [12]. However, this simple approach is solely based on specific statistical data and therefore not repeatable for other conditions. Moreover, simple analytical approaches have been used in the modelling of a solar power-integrated distribution system [13]. A previous study has incorporated the reliability effect of the PV system protection device (i.e. fuse) [14]. The fault tree analysis has also been used for systematic identification due to the various operating states of the PV system [15].

Given the stochastic nature of solar radiation, a simulation-based reliability study, especially a Monte Carlo simulation, is more effective than the previously mentioned methods. The failure rates of various PV system components have been modelled on the basis of weather conditions [16], such as temperature and irradiance [17], [18]. Wind and load data are also included to obtain an accurate PV power output model for robust reliability analyses [19]–[21]. The PV system has also been modelled on the basis of the clearness index, which follows the beta probability distribution function [22].

The associate editor coordinating the review of this manuscript and approving it for publication was Feng Wu.

The aforementioned factors lay the foundation for the reliability studies of smart grid systems integrated with various forms of RE, especially solar energy, with the consideration of the uncertainty in ambient temperature [23], [24] and demand–response [25]. However, the modelling of internal PV components is neglected, and the previous advances in the corresponding reliability modelling have never been improved. On this basis, various models have been proposed. The effect of the mission profile resolution on the failure rate of the PV system inverter was investigated to resolve this issue [26]. The Markov model was utilised to identify and model the various states of the PV components [27]. This technique has been extended to include the stochastic property of solar radiation data and the effect of intermittent faults on PV system components [28], [29].

However, several drawbacks have been identified in the aforementioned methods. Firstly, these methods ignore the reliability modelling of major PV system components (e.g. panels, converters, inverters, fuses and connectors) despite the unique failure rates and different responses to various environmental conditions [11]. Ignoring these characteristics and lumping the components into a single part is unrealistic and results in a large bias in the reliability evaluation of PV systems. Secondly, fixed failure rates of the PV system components are arbitrarily used [8]. The fixed failure rate assumes that the weather parameters are constant over time by taking the average values. However, this assumption results in the unrealistic evaluation of system reliability in which the components are differently affected by the varying weather conditions over the year. Moreover, the components show higher failure probability under extreme weather in comparison with normal weather conditions.

To address the identified drawbacks, this study proposes a new method for the reliability modelling of PV systems. The proposed system details the modelling of the PV components and considers all neglected factors identified in the second drawback. Moreover, a realistic PV system structure is considered when determining the chronological state transition sequence of the system. A new and robust solar radiation model from previously published works is also utilised in the reliability model of the proposed PV system. The main outcome of the proposed reliability model is the time-varying failure rates of the PV system, which is then used to determine the PV power output.

The remainder of this paper is organised as follows: Section II describes the proposed PV system reliability model. Section III analyses the proposed model and presents the results. Section IV provides the conclusions.

II. METHODOLOGY

A. PV SYSTEM STRUCTURE

The proposed three-phase grid-connected PV system is shown in Fig. 1 [16], [30]. The maximum capacity of the proposed system is 1 MW, which is generated by 4000 ND-R250A5 PV panels and separated into 10 arrays. Each

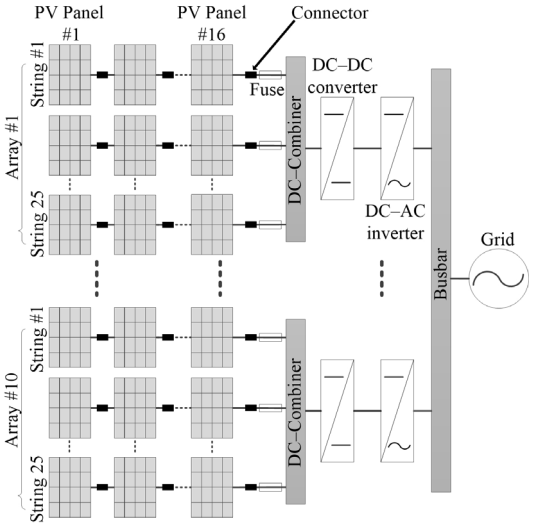

FIGURE 1. Structure of a typical PV power system.

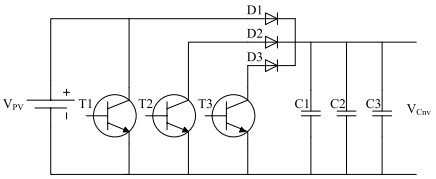

FIGURE 2. Three-leg DC-DC converter.

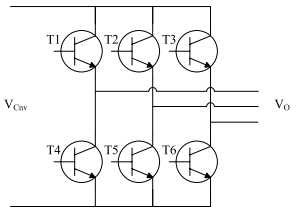

FIGURE 3. Three-phase inverter.

array is further separated into 25 parallel strings in which each string is a series connection of 16 PV panels. Each panel has a connector, and each string is ended with a fuse that is fitted into another connector. The fuse is connected to the DC combiner box with an output voltage level boosted by a three-leg DC–DC converter to match the input voltage requirement of the three-phase inverter. The power capacity of the converter is 100 kW, with nominal input and output voltages of 500 and 620 V, respectively. The physical structure of the three-leg converter is shown in Fig. 2. Each leg comprises a transistor, a diode and a capacitor [8]. The power capacity of the three-phase inverter is the same as that of the converter and has nominal input and output voltages of 620 and 380 V, respectively [8]. The physical structure of the inverter comprises transistors only (Fig. 3). Through the inverter, the DC power generated by the PV panels is converted into AC form before injection into the grid via a fully reliable busbar.

Although the proposed PV system has a specific number of components, the presented architecture in Figs. 1–3 represents a typical design of the PV system. Hence, the proposed reliability model can still be applied to any PV system with different numbers of components.

B. PV SYSTEM FAILURE RATE MODEL

As mentioned in the introduction, the failure rates used in the current reliability studies of PV systems are fixed on the basis of the statistical records of specific environmental conditions. Hence, reusing the same failure rates in the modelling of the PV system at different environmental conditions is not a reflection of the actual reliability behaviour of the PV system. As a countermeasure, this study uses physics-of-failure theory used in the FIDES guide [9] as the methodology for modelling the major components of the PV system described in Section II.A. The guide considers physical and technological factors, thermal and mechanical overstresses, manufacturing properties and the mission profile, which is a systematic manner of describing and organising all operations performed by the system [31], [32]. An overview of the proposed PV system failure rate model is shown in Fig. 4. Where solar radiation (E), temperature (T) and humidity (H) are the three major inputs of the proposed model.

Firstly, modelling the failure rates of the PV system requires solar radiation, temperature and humidity data, which are all obtained from the State University of New York Project [33]. The data obtained from two locations, namely, Aceh, Indonesia (5.05°N, 97.45°E) and Vancouver, Canada (49.25°N, 123.1°W), from 2000 to 2014 are recorded hourly. Solar radiation is modelled on the basis of the previously published method [34] and simulated for 10,000 years. The hourly average of the solar radiation data is obtained from this model and grouped in accordance with the respective months. The number of year simulated is to ensure that the variation coefficient of the hourly solar radiation data is smaller than 5%. The obtained temperature and humidity data are constant over the entire period and can be reasonably assumed for repetition in the future.

In the second step, the mission profile of the PV system is defined on the basis of the level of the generated PV power. This basis is reasonable because the PV system is only used to convert solar radiation into electrical power; no mechanical movement in the system requires a sophisticated mission profile. The PV power level and the mission profile are separated into 11 levels of equal 10% intervals starting from the dormant state where no power output is available for each day. The PV power output of a single PV panel can be calculated as

$$\Psi^{\alpha} = \frac{E^{\alpha}}{E_0} P_{m0} \left[1 + \gamma_P (T^{\alpha} - T_0)\right] \tag{1}$$

where Ψ^{α}, E^{α} and T^{α} are the hourly PV power generation from a single PV panel, the hourly incident solar radiation on a PV panel, and temperature of the α^{th} day, respectively; E_0, P_{m0} and T_0 are the solar irradiance, PV panel rated power and temperature at standard test conditions; and γ_P is the temperature coefficient of the power parameter [10]. At each hour of the day, (1) is obtained, and the mission profile of the day is identified. An example of the PV panel mission profile of the 15th day in January is presented in Fig. 5, where P_{max} denotes the maximum PV power generated by a single PV panel over the respective month. The values of Ψ^{α}, T^{α} and humidity H^{α} from the same month are separately combined to form the matrix below.

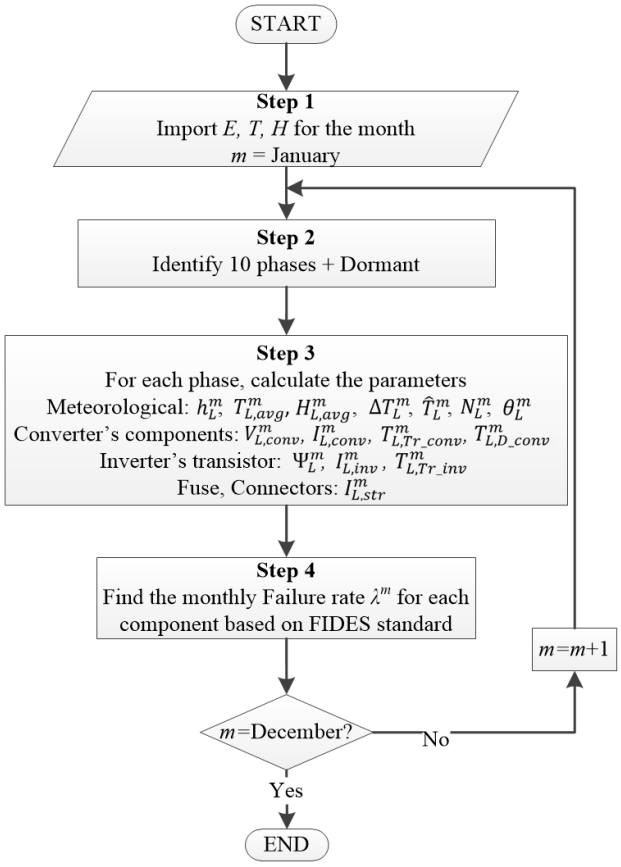

FIGURE 4. Proposed PV system failure rate model.

$$\Psi^m, T^m \text{ or } H^m = \begin{bmatrix} x_1^1 & \cdots & x_j^1 & \cdots & x_{24}^1 \\ x_1^2 & \cdots & x_j^2 & \cdots & x_{24}^2 \\ \vdots & \ddots & \vdots & \ddots & \vdots \\ x_1^{\alpha} & \cdots & x_j^{\alpha} & \cdots & x_{24}^{\alpha} \end{bmatrix} \tag{2}$$

where Ψ^m, T^m and H^m are the matrices containing all values of Ψ^{α}, T^{α} and H^{α}, respectively, in the m^{th} month; x is either Ψ^{α}, T^{α} or H^{α}; and the subscript j denotes the hour position of the input x.

From (2), all index pairs (α, j) between the power level L and $L-1$ are determined as

$$k_L^m = \left[\alpha, j \middle| (L-1)\frac{P_{max}}{10} < x_j^{\alpha} \leq L\frac{P_{max}}{10}\right] \tag{3}$$

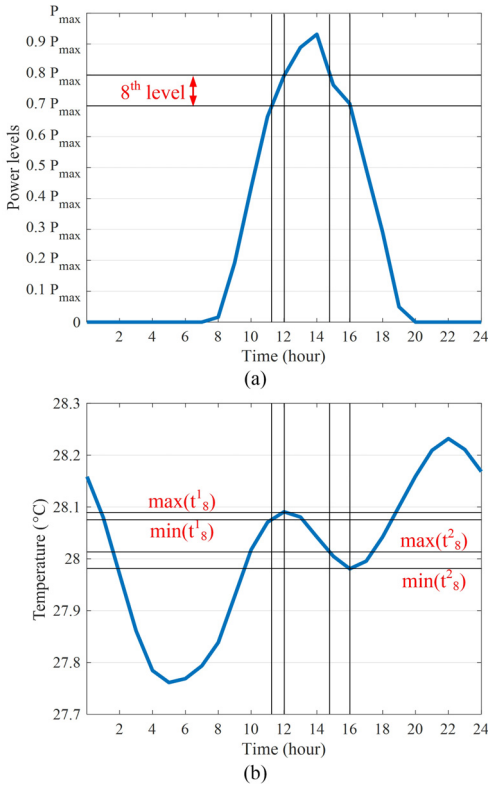

FIGURE 5. Mission profile of the PV system on January 15 showing (a) output power and (b) temperature profiles.

where k_L^m is the set of all index pairs between L and $L-1$ for Ψ^m, T^m and H^m. The functions $\Psi^m\left(k_L^m\right)$, $T^m\left(k_L^m\right)$ and $H^m\left(k_L^m\right)$ respectively represent all PV power output, temperature and humidity values of the L^{th} level in the m^{th} month.

In the third step, several key parameters are derived. From (3), the size of k_L^m, which is the number of elements (numel), is obtained. Then, the number of hours, which is denoted as h_L^m, is determined as

$$h_L^m = \text{numel}\left(k_L^m\right) \tag{4}$$

From (2) and (3), the average values of the weather conditions are calculated as

$$T_{L,avg}^m = \text{mean}\left(T^m\left(k_L^m\right)\right) \tag{5}$$
$$H_{L,avg}^m = \text{mean}\left(H^m\left(k_L^m\right)\right) \tag{6}$$

where $T_{L,avg}^m$ and $H_{L,avg}^m$ are the respective average values of the temperature and humidity of the L^{th} level in the m^{th} month.

A cycle z is counted when the PV power output enters $L-1$ and exits L, or vice versa. Subsequently, the total number of cycles of the L^{th} level in the m^{th} month N_L^m is determined by summing all cycles of the respective level.

$$N_L^m = \text{numel(Z)} \tag{7}$$

where $1 \le \text{Z} \le z$. Then, the average cycle duration of the L^{th} level in the m^{th} month is determined as

$$\theta_L^m = \frac{h_L^m}{N_L^m} \tag{8}$$

where θ_L^m is the average cycle duration of the L^{th} level in the m^{th} month.

The temperature difference of the corresponding cycle is determined and repeated for all cycles by tracing the identified cycles onto the temperature curves. Subsequently, the average temperature difference of the L^{th} level in the m^{th} month is determined as

$$\Delta T_L^m = \frac{1}{N_L^m}\sum_{z=1}^{N_L^m}\left(\max\left(t_L^z\right) - \min(t_L^z)\right) \tag{9}$$

where t_L^z is the temperature values of the z^{th} cycle and L^{th} level.

From (7) and (9), the average maximum cycle temperature of the L^{th} level in the m^{th} month $\hat{T}_L^m$ is calculated as

$$\hat{T}_L^m = \frac{1}{N_L^m}\sum_{z=1}^{N_L^m}\max\left(t_L^z\right) \tag{10}$$

Next, the average power output generated by a PV panel of the L^{th} level in the m^{th} month Ψ_L^m is determined as

$$\Psi_L^m = \text{mean}(\Psi^m\left(k_L^m\right)) \tag{11}$$

In consideration of the converter and inverter of the PV system running at efficiencies of $X\%$ and $Y\%$, respectively, with respective nominal output voltages of 620 and 380 V, the corresponding output currents are determined as

$$I_{L,conv}^m = \frac{\Psi_L^m \times C_P \times C_S}{620} \times \frac{X}{100} \tag{12}$$
$$I_{L,inv}^m = \frac{\Psi_L^m \times C_P \times C_S}{380} \times \frac{X}{100} \times \frac{Y}{100} \tag{13}$$

where C_P and C_S are the total number of PV panels connected in parallel and series forming an array, respectively.

Lastly, the junction temperatures of every diode and transistor in the transistors of all converters and inverters, denoted as T_{L,D_conv}^m, T_{L,Tr_conv}^m and T_{L,Tr_inv}^m, are determined on the basis of the methods in [35], [36]. The current in each string $I_{L,str}^m$ of the L^{th} level is determined to be equal to the PV panel current output.

$$I_L^m = \frac{\Psi_L^m}{\text{V}_L^m} \tag{14}$$

where V_L^m is the terminal voltage of the PV panel of the respective level; this voltage is highly dependent on the level's temperature $T_{L,avg}^m$.

$$\text{V}_L^m = V_0\left[1 + \gamma_V(T_{L,avg}^m - T_0)\right] \tag{15}$$

where V_0 is the maximum power point voltage of the PV panel under standard test conditions, and γ_V is the temperature coefficient of the voltage parameter [37].

In the fourth step, the failure rate of any PV system component in the m^{th} month, λ^m, is determined as [9]

$$\lambda^m = \lambda^m_{Phy} \Pi_{PM} \Pi_{Process} \tag{16}$$

where λ^m is the failure rate of either the transistors, diodes, capacitors, connectors or fuses, which collectively form the PV system structure in Section II.A, λ^m_{Phy} is the physical contributing factor of the reliability of the previously mentioned component in the m^{th} month, and Π_{PM} and $\Pi_{Process}$ are the quality and technical conditions of the manufacturing and usage processes of the component, respectively.

λ^m_{Phy} of the component is calculated for every month as a function of the set of weather parameters Ω_w and the set of parameters associated with either the converter transistor Ω^{conv}_{Tr}, converter diode Ω^{conv}_{D}, converter capacitor Ω^{conv}_{C}, inverter transistor Ω^{inv}_{Tr}, PV connector Ω_{Con}, fuse connector Ω_{Fcon} or fuse Ω_F.

$$\lambda^m_{Phy} = f\left(\Omega_w, \begin{pmatrix} \Omega^{conv}_{Tr}, \Omega^{conv}_{D}, \Omega^{conv}_{C}, \Omega^{inv}_{Tr}, \\ \Omega_{Con}, \Omega_{Fcon} \text{ or } \Omega_F \end{pmatrix}\right) \tag{17}$$

where

$$\Omega_w = f\left(h^m_L, T^m_{L,avg}, H^m_{L,avg}, N^m_L, \theta^m_L, \Delta T^m_L, \hat{T}^m_L\right) \tag{18}$$

$$\Omega^{conv}_{Tr} = f\left(V^m_{L,conv}, I^m_{L,conv}, T^m_{L,Tr\_conv}\right) \tag{19}$$

$$\Omega^{conv}_{D} = f\left(V^m_{L,conv}, I^m_{L,conv}, T^m_{L,D\_conv}\right) \tag{20}$$

$$\Omega^{conv}_{C} = f\left(V^m_{L,conv}\right) \tag{21}$$

$$\Omega^{inv}_{Tr} = f\left(\Psi^m_L, I^m_{L,inv}, T^m_{L,Tr\_inv}\right) \tag{22}$$

$$\Omega_{Con}, \Omega_{Fcon} \text{ and } \Omega_F = f\left(I^m_{L,str}\right) \tag{23}$$

where $V^m_{L,conv}$ is the voltage at the converter terminal. Equations (16) to (23) are long and therefore not expanded in this work due to page limitation, but the details of these equations can be found in [9]. The repair rates of all components specified in (19)–(23) from [8] are considered constant because these rates are rarely affected by environmental conditions.

C. PV SYSTEM POWER OUTPUT MODEL

Based on the failure rates obtained in Section II.B, the step-by-step process for determining the hourly PV system output is presented in Fig. 6 and described as follows.

Step 1: The sequential Monte Carlo Simulation (SMCS) is initialised at $y = 1$ and $t = 1$, which represent the simulation year and hour of the year, respectively.

Step 2: At the t^{th} hour, the failure rate of a component is denoted as $\lambda(t)$. An example of the failure rate propagation of the converter transistor is shown in Fig. 7. Considering that the failure rate follows an exponential distribution, the probability density function (PDF) and cumulative distribution function (CDF) of the component are determined as

$$f(t) = \lambda(t)\, e^{-\lambda(t)t} \tag{24}$$

$$F_t(T) = \sum_{t=hr_i}^{T} f(t) \tag{25}$$

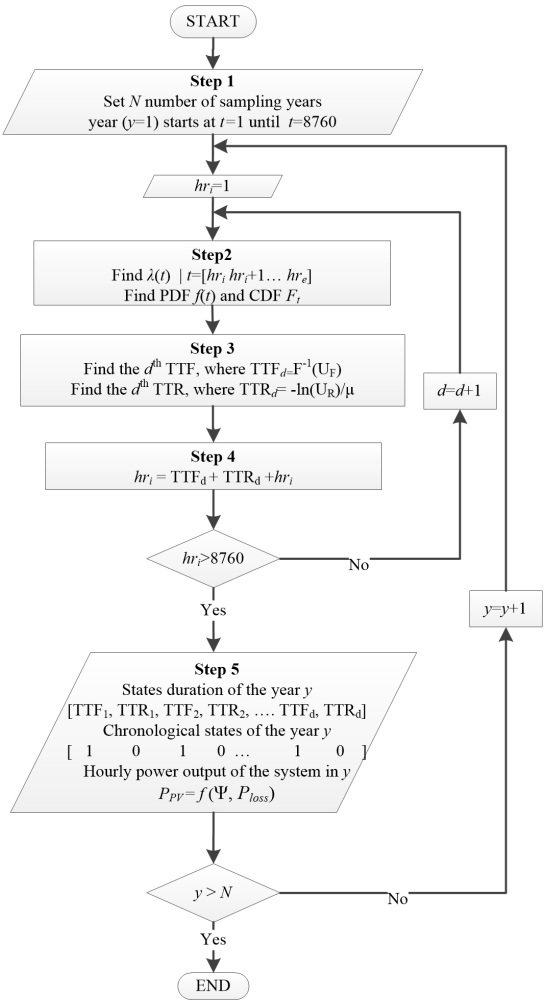

FIGURE 6. Failure rates of the PV system array in Aceh and Vancouver.

At the start of the simulation, when $t = 1$, the input range of $f(t)$ is $1 \le t \le 8760$ or generally $hr_i \le t \le hr_e$. However, when $t = hr_i = 50$, the input range is broken down into two parts when t has progressed beyond the final hour: $50 \le t \le 8760$ and $1 \le t \le 49$. The second part restarts from the beginning as the first interval exhausted from all hours of the year to maintain a full period of 8760 h. Then, T is defined as

$$T = \begin{cases} 1 \le t \le 8760 & hr_i = 1 \\ hr_i \le t \le 8760 + 1 \le t \le hr_i - 1 & hr_i > 1 \end{cases} \tag{26}$$

Step 3: A random number U_f is generated. The d^{th} time-to-failure (TTF) of the component is determined by applying the inverse transform method on the CDF obtained in the previous step, as the following:

$$\text{TTF}_d = F_t^{-1}\left(U_f\right) \tag{27}$$

Moreover, the time-to-repair (TTR) of the component is always directly determined using another random number U_r because the repair rate of the component μ is considered

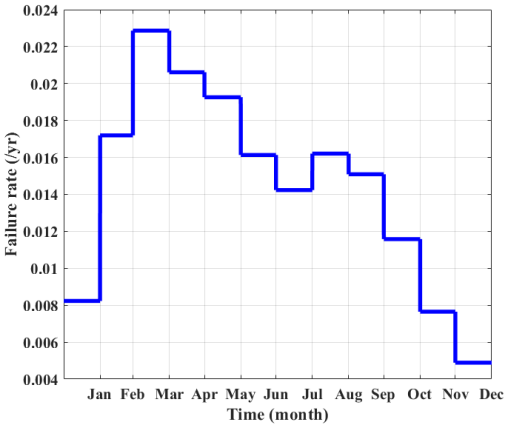

FIGURE 7. Example of the time-varying failure rate of a transistor operating in Aceh.

constant over time [38], as the following:

$$\mathrm{TTR}_d = -\frac{1}{\mu} ln\,(U_r) \tag{28}$$

Step 4: After each cycle ($\mathrm{TTF}_d + \mathrm{TTR}_d$), a new TTF is generated on the basis of the new CDF of the failure rates. Take the sample in *Step 2* as an example; if the component is restored at $t = 50$, then the new TTF is generated on the basis of the new CDF determined from the failure rates ranging from the 50^{th} to the 8760^{th} hour and restarts from the 1^{st} until the 49^{th} hour. Then, a new TTR is generated on the basis of (28) using a new U_r. The entire process in *Step 3* is repeated until the complete status of the component is obtained for 8760 h.

Step 5: The chronological states of all PV components in the sampling year y are obtained on the basis of the up–down cycles generated in *Step 4*. The processes from *Steps 1–5* are repeated until the number of the sampling year N is achieved. N should be sufficiently large to ensure that the variation coefficient of the expected PV power output is less than 5% before ending the SMCS.

The power capacity of the PV system is determined on the basis of the status combinations of all components. In consideration of which component is not functioning, the failure category of the nonfunctioning component is identified (Table 1) on the basis of the PV system structure presented in Fig. 1. Table 1 shows that a fuse, connector or fuse–connector failure only disconnects the respective string of the PV system, whereas a converter or inverter failure disconnects an entire array of the PV system. Moreover, the latter two are considered failures if a single component in the respective systems is not functioning (Figs. 2 and 3).

The total power generation of the PV system is a function of the internal structure of the system. The proposed PV system has 10 arrays and 25 strings; thus, the fraction of power loss P_{loss} based on the failure category is determined by considering that the total capacity of the PV system is equally shared amongst the strings. Then, the hourly power

TABLE 1. Failure categories of the PV system components.

Component	Category	P_{loss}
Fuse	String	$1/(25 \times 10)$
Connector	String	$1/(25 \times 10)$
Fuse-connector	String	$1/(25 \times 10)$
Inverter	Array	1/10
Converter	Array	1/10

output of the PV system P_{PV} is determined as

$$P_{PV} = \left[\sum_{i\in\Omega_A}\left(1 - P_{loss,i}\right) + \sum_{\substack{j\in\Omega_S \\ \Omega_S\notin\Omega_A}}\left(1 - P_{loss,j}\right)\right] \times \Psi \times C_P \times C_S \times C_A \tag{29}$$

where Ψ is the hourly PV system power output determined in (1), Ω_A is the set of array failure categories, Ω_S is the set of string failure categories in which the arrays containing the affected strings do not entirely fail, and C_A is the number of arrays in the system.

III. RESULTS AND DISCUSSIONS

The proposed time-varying failure rate model is applied using the weather conditions in Aceh and Vancouver, and the results are compared with the conventional yearly failure rate model [8]. The results from the two locations are compared in terms of failure rate values, availability, PDF and solar output energy. Sensitivity studies are also performed by varying the solar radiation, temperature and humidity to evaluate the response of the failure rate.

A. FAILURE RATE AND AVAILABILITY

On the basis of the PV system structure and failure rate model presented in Sections II.A and II.B and the collected weather data, the failure rates of the PV arrays for every month (assuming that all arrays are identical) are obtained using (30) and (31) [39].

When the PV components are connected in series, the equivalent series system failure rate is expressed as

$$\lambda_s = \sum_{i=1}^{N_s} \lambda_i \tag{30}$$

where λ_s is the failure rate of a series system, and N_s is the number of components in the series system.

When the PV components are connected in parallel, the equivalent parallel system failure rate is determined as

$$\lambda_p = \prod_{i=1}^{N_p} \lambda_i \sum_{j=1}^{\binom{N_p}{2}} \Delta_j \tag{31}$$

where λ_p is the failure rate of the parallel system, and Δ is the multiplication of the repair durations (reciprocal of μ) of

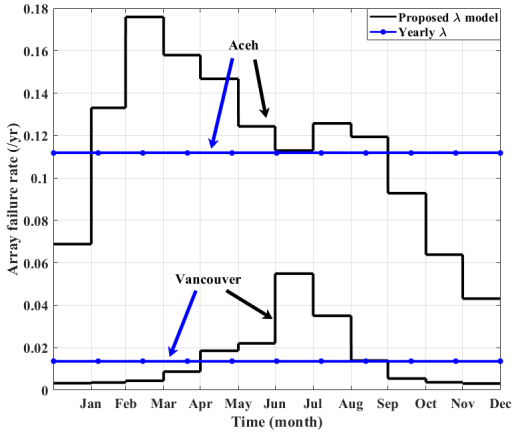

FIGURE 8. Failure rates of the PV system array in Aceh and Vancouver.

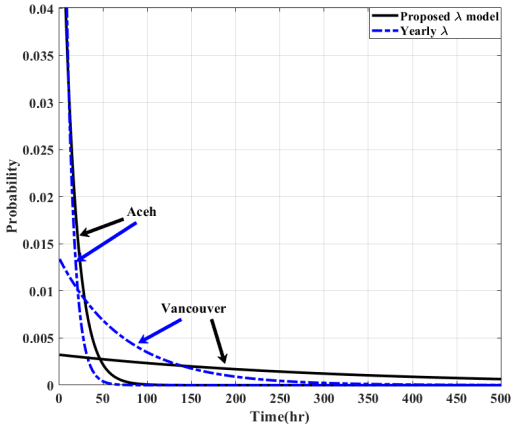

FIGURE 9. Failure probability of the PV system array in Aceh and Vancouver.

the two-element combination drawn from N_p, which is the number of components in the parallel system.

On the basis of the various combinations of (30) and (31), the equivalent monthly (proposed model) and yearly [8] failure rates of the PV array are depicted in Fig. 8. Considerable differences are observed in the failure rates of both locations every month. These differences indicate that the environmental conditions of the PV system exert a considerable influence on the reliability of the components. Neglecting the effects of the environmental conditions results in the same failure rates for both locations despite the distinctive weather conditions. This phenomenon might eventually lead to a drastic misrepresentation of the actual failure rates of arrays. On average, the failure rates in Vancouver are lower than those in Aceh by approximately 87%. Fig. 8 also shows the yearly failure rates of both locations. The comparison of these values with those of the monthly failure rates indicates that the proposed model can accurately represent the array failures at various months in a year. On the one hand, although the yearly failure rate in Aceh approximates the monthly failure rate in July, this value is significantly different from that of the other months, especially that in December, which is the largest at approximately 62%. In addition, the percentage difference between the monthly and yearly failure rates in Aceh is approximately 28% on the average. On the other hand, the largest deviation between the monthly and yearly failure rates in Vancouver is observed in July at approximately 305%. The average percentage difference is approximately 85%, which is 57% higher than that in Aceh. The comparison of the overall percentage difference between the monthly and yearly failure rates in Vancouver and Aceh shows that the weather conditions in Aceh fluctuate less and are more stable than that in Vancouver, resulting in an overall low percentage difference in Aceh. This phenomenon can be attributed to Aceh's tropical climate, which fluctuates less than the seasonal weather in Vancouver. The PDF of the failure probability of the two locations is plotted in Fig. 9. The average percentage difference between the PDFs calculated from the monthly and yearly failure rates in Vancouver is approximately 0.016%, whereas

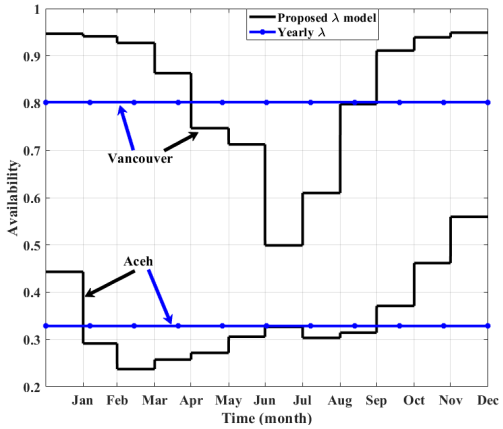

FIGURE 10. Availability of the PV system array in Aceh and Vancouver.

that in Aceh is approximately 0.006%, which is lower than Vancouver by approximately 62.5%. This trend is consistent with the results illustrated in Fig. 8.

The availability values of the PV array in both locations are calculated in accordance with the failure rates (Fig. 10). The availabilities in Vancouver are higher than those in Aceh regardless of the calculation based on the monthly or yearly failure rates. This result is reasonable because the failure rates in the former are lower than those in the latter. On average, the availabilities in Vancouver are higher than those in Aceh by approximately 138% compared with the monthly values. When the yearly and monthly availabilities in each location are compared, the average percentage difference in Aceh is larger than that in Vancouver by approximately 21% and 15%, respectively. This finding is in contrast to the previously mentioned comparison results based on failure rates. The average percentage difference in Aceh is lower than that in Vancouver due to the stable tropical climate in Aceh. This finding indicates that the characteristic of availability is not necessarily similar to that of failure rate due to the additional influence of the repair rate [39] when determining the overall

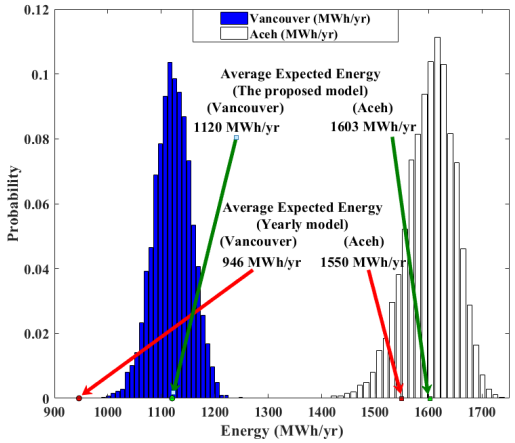

FIGURE 11. Energy outputs of the PV system generated on the basis of the monthly and yearly failure rates.

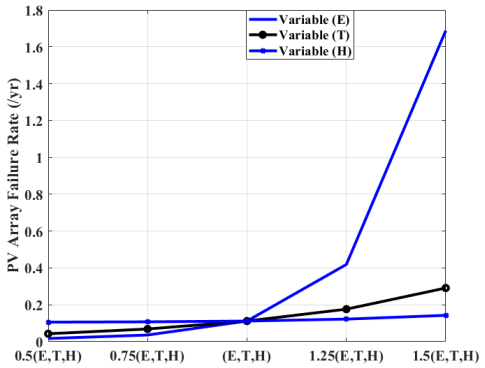

FIGURE 12. Effects of solar radiation, temperature and humidity on the failure rates of the PV system.

availability of the PV array.

$$\mu_s = \frac{\lambda_s}{\sum_{i=1}^{N_s} \lambda_i \mu_i} \tag{32}$$

$$\mu_p = \sum_{i=1}^{N_p} \mu_i \tag{33}$$

where μ_s and μ_p are the repair rate of the series- and parallel-connected systems, respectively. Furthermore, the repair rate of a series system is affected by the failure rates.

B. EXPECTED ENERGY OUTPUT

In this section, the output solar energy of the considered 1 MW PV system (Section II.A) in both locations is determined on the basis of the respective monthly and yearly failure rates. The probability distribution of all simulated output energies and the expected values after the convergence of the SMCS are presented in Fig. 11. The results demonstrate that the expected energy output in Aceh is higher than that in Vancouver by approximately 43% and 64% based on the monthly and yearly failure rates, respectively. The difference between the two values indicates that using the yearly rates, instead of the proposed monthly failure rates, overestimates the difference of the expected solar energy output between the two locations by approximately 21%.

The comparison of the expected energy output based on the proposed monthly and yearly failure rates for each location implies that the proposed model has an expected energy yield increment of approximately 3.4% if the conventional yearly failure rate is used in Aceh. By contrast, the difference in Vancouver is prevalent at approximately 18%. In other words, using the yearly failure rate underestimates the energy output capacity of the PV system, especially in high-latitude locations, such as Vancouver, where the weather conditions often change. Although the weather conditions in Vancouver are more desirable than those in Aceh in terms of the reliable operations of the PV system (Fig. 8), the expected energy output in Vancouver is approximately 30% lower than that of Aceh based on the proposed monthly failure rate due to the high intensity and availability of solar radiation in Aceh.

C. SENSITIVITY STUDY

In this section, the three major inputs of the proposed monthly failure rate E, T and H are individually varied by a factor of 0.5 until 1.5 with an increment of 0.25 to identify the critical input. The monthly failure rates of the PV array in Aceh and the average values are presented in Fig. 12. The results clearly demonstrate that E has the greatest effect on failure rate, followed by T and H. At 1.5 times the original value of E, the failure rate increases by approximately 14 times. When the same factor is applied to T and H, the failure rate increases by approximately 1.6 and 0.27 times, respectively. In conclusion, E is the most critical influencing factor of the failure rate of the array and the entire PV system.

IV. CONCLUSION

This study presented a new failure rate model for PV systems by considering environmental weather conditions, PV system architecture, interactions of PV components with the weather conditions, manufacturing quality and materials used. The key weather parameters included solar radiation, temperature and humidity. The monthly failure rates of the components of the PV system (e.g. fuses, connectors, transistors, diodes and capacitors) were determined and combined to identify the final failure rate of the entire PV system. Results from the proposed model showed that the failure rates in most months were significantly different from the conventional yearly failure rate. In addition, the monthly failure rates fluctuated above and below the yearly failure rates. Hence, using a fixed failure rate for the entire year could yield inaccuracy and bias in the reliability analyses. The proposed model was also tested under two different climate locations: tropical and seasonal. The comparison emphasised that the difference between the monthly and yearly failure rates in locations with seasonal climate is more significant than those with tropical climate. Moreover, similar outcomes were observed when the expected energy outputs of the same PV system used in

the two locations were compared. Sensitivity analyses were performed to identify the critical weather parameters that affect the failure rates of the PV system. The analysis result indicated that solar radiation demonstrated the greatest effect amongst the three parameters.

REFERENCES

[1] C. Pascal and C. Morgan, "Global energy trends a new historic high in energy consumption and CO_2 emissions," Enerdata, Grenoble, France, Tech. Rep., 2018. [Online]. Available: https://www.enerdata.net

[2] M. Drechsler, J. Egerer, M. Lange, F. Masurowski, J. Meyerhoff, and M. Oehlmann, "Efficient and equitable spatial allocation of renewable power plants at the country scale," *Nature Energy*, vol. 2, no. 9, p. 17124, 2017.

[3] L. Sussams and J. Leaton, "Expect the unexpected: The disruptive power of low-carbon technology," Carbon Tracker Initiative, London, U.K., Tech. Rep., 2017.

[4] H. Abunima, J. Teh, C.-M. Lai, and H. Jabir, "A systematic review of reliability studies on composite power systems: A coherent taxonomy motivations, open challenges, recommendations, and new research directions," *Energies*, vol. 11, no. 9, p. 2417, Sep. 2018.

[5] D. S. Pillai and N. Rajasekar, "A comprehensive review on protection challenges and fault diagnosis in PV systems," *Renew. Sustain. Energy Rev.*, vol. 91, pp. 18–40, Aug. 2018.

[6] D. K. Khatod, V. Pant, and J. Sharma, "Analytical approach for well-being assessment of small autonomous power systems with solar and wind energy sources," *IEEE Trans. Energy Convers.*, vol. 25, no. 2, pp. 535–545, Jun. 2010.

[7] R. M. Moharil and P. S. Kulkarni, "Reliability analysis of solar photovoltaic system using hourly mean solar radiation data," *Sol. Energy*, vol. 84, no. 4, pp. 691–702, Apr. 2010.

[8] N. Shahidirad, M. Niroomand, and R.-A. Hooshmand, "Investigation of PV power plant structures based on Monte Carlo reliability and economic analysis," *IEEE J. Photovolt.*, vol. 8, no. 3, pp. 825–833, Apr. 2018.

[9] *FIDES Guide 2009, Edition A: Reliability Methodology for Electronic Systems*, FIDES Group, Montpellier, France, 2010.

[10] S. E. De Leon-Aldaco, H. Calleja, and J. Aguayo Alquicira, "Reliability and mission profiles of photovoltaic systems: A FIDES approach," *IEEE Trans. Power Electron.*, vol. 30, no. 5, pp. 2578–2586, May 2015.

[11] S. De Leon, H. Calleja, and J. Mina, "Reliability of photovoltaic systems using seasonal mission profiles and the FIDES methodology," *Microelectron. Rel.*, vol. 58, pp. 95–102, Mar. 2016.

[12] H. Li, J. Ding, J. Huang, Y. Dong, and X. Li, "Reliability evaluation of PV power systems with consideration of time-varying factors," *J. Eng.*, vol. 2017, no. 13, pp. 1783–1787, Jan. 2017.

[13] K. Zou, A. P. Agalgaonkar, K. M. Muttaqi, and S. Perera, "An analytical approach for reliability evaluation of distribution systems containing dispatchable and nondispatchable renewable DG units," *IEEE Trans. Smart Grid*, vol. 5, no. 6, pp. 2657–2665, Nov. 2014.

[14] I.-S. Bae and J.-O. Kim, "Reliability evaluation of customers in a microgrid," *IEEE Trans. Power Syst.*, vol. 23, no. 3, pp. 1416–1422, Aug. 2008.

[15] A. Ahadi, N. Ghadimi, and D. Mirabbasi, "Reliability assessment for components of large scale photovoltaic systems," *J. Power Sources*, vol. 264, pp. 211–219, Oct. 2014.

[16] P. Zhang, Y. Wang, W. Xiao, and W. Li, "Reliability evaluation of grid-connected photovoltaic power systems," *IEEE Trans. Sustain. Energy*, vol. 3, no. 3, pp. 379–389, Jul. 2012.

[17] I. Yahyaoui, G. Tina, M. Chaabene, and F. Tadeo, "Design and evaluation of a renewable water pumping system," *IFAC-PapersOnLine*, vol. 48, no. 30, pp. 462–467, 2015.

[18] H. Baghaee, M. Mirsalim, G. Gharehpetian, and H. Talebi, "Reliability/cost-based multi-objective Pareto optimal design of stand-alone wind/PV/FC generation microgrid system," *Energy*, vol. 115, pp. 1022–1041, Nov. 2016.

[19] Z. Qin, W. Li, and X. Xiong, "Incorporating multiple correlations among wind speeds, photovoltaic powers and bus loads in composite system reliability evaluation," *Appl. Energy*, vol. 110, pp. 285–294, Oct. 2013.

[20] M. Mosadeghy, R. Yan, and T. K. Saha, "A time-dependent approach to evaluate capacity value of wind and solar PV generation," *IEEE Trans. Sustain. Energy*, vol. 7, no. 1, pp. 129–138, Jan. 2016.

[21] M. Mosadeghy, R. Yan, and T. K. Saha, "Impact of PV penetration level on the capacity value of South Australian wind farms," *Renew. Energy*, vol. 85, pp. 1135–1142, Jan. 2016.

[22] M. Hamzeh, B. Vahidi, and H. Askarian-Abyaneh, "Reliability evaluation of distribution transformers with high penetration of distributed generation," *Int. J. Elect. Power Energy Syst.*, vol. 73, pp. 163–169, Dec. 2015.

[23] H. Hashemi-Dezaki, H. Haeri-Khiavi, and H. Askarian-Abyaneh, "Impacts of direct cyber-power interdependencies on smart grid reliability under various penetration levels of microturbine/wind/solar distributed generations," *IET Gener., Transmiss. Distrib.*, vol. 10, no. 4, pp. 928–937, Mar. 2016.

[24] H. Gunduz and D. Jayaweera, "Reliability assessment of a power system with cyber-physical interactive operation of photovoltaic systems," *Int. J. Electr. Power Energy Syst.*, vol. 101, pp. 371–384, Oct. 2018.

[25] S. M. Nosratabadi, R.-A. Hooshmand, E. Gholipour, and S. Rahimi, "Modeling and simulation of long term stochastic assessment in industrial microgrids proficiency considering renewable resources and load growth," *Simul. Model. Pract. Theory*, vol. 75, pp. 77–95, Jun. 2017.

[26] A. Sangwongwanich, D. Zhou, E. Liivik, and F. Blaabjerg, "Mission profile resolution impacts on the thermal stress and reliability of power devices in PV inverters," *Microelectron. Rel.*, vols. 88–90, pp. 1003–1007, Sep. 2018.

[27] T. Adefarati and R. Bansal, "Reliability and economic assessment of a microgrid power system with the integration of renewable energy resources," *Appl. Energy*, vol. 206, pp. 911–933, Nov. 2017.

[28] B. Cai, Y. Liu, Y. Ma, L. Huang, and Z. Liu, "A framework for the reliability evaluation of grid-connected photovoltaic systems in the presence of intermittent faults," *Energy*, vol. 93, pp. 1308–1320, Dec. 2015.

[29] T. Adefarati and R. Bansal, "Reliability assessment of distribution system with the integration of renewable distributed generation," *Appl. Energy*, vol. 185, pp. 158–171, Jan. 2017.

[30] D. S. Pillai, F. Blaabjerg, and N. Rajasekar, "A comparative evaluation of advanced fault detection approaches for PV Systems," *IEEE J. Photovolt.*, vol. 9, no. 2, pp. 513–527, Mar. 2019.

[31] J. Marin and R. Pollard, "Experience report on the FIDES reliability prediction method," in *Proc. Annu. Rel. Maintainab. Symp.*, Mar. 2005, pp. 8–13.

[32] M. Held and K. Fritz, "Comparison and evaluation of newest failure rate prediction models: FIDES and RIAC 217Plus," *Microelectron. Rel.*, vol. 49, nos. 9–11, pp. 967–971, Sep. 2009.

[33] *SUNY India Direct Normal Irradiance*, NREL, Golden, CO, USA, 2015.

[34] H. Abunima, J. Teh, and H. J. Jabir, "A new solar radiation model for a power system reliability study," *IEEE Access*, vol. 7, pp. 64758–64766, 2019.

[35] A. Wintrich, U. Nicolai, W. Tursky, and T. Reimann, *Application Manual Power Semiconductors*. Ilmenau, Germany: ISLE Verlag, 2015.

[36] SEMIKRON. *SemiSel Simulation: Step By Step Design*. Accessed: Jan. 17, 2020. [Online]. Available: https://www.semikron.com/service-support/semisel-simulation.html

[37] C. S. Solanki, *Solar Photovoltaic Technology and Systems: A Manual for Technicians, Trainers and Engineers*. New Delhi, India: PHI Learning, 2013.

[38] J. Teh and I. Cotton, "Reliability impact of dynamic thermal rating system in wind power integrated network," *IEEE Trans. Rel.*, vol. 65, no. 2, pp. 1081–1089, Jun. 2016.

[39] R. Billinton and R. N. Allan, *Reliability Evaluation of Engineering Systems*. New York, NY, USA: Springer, 1992.

HAMZA ABUNIMA received the B.S. degree in electrical engineering from the Islamic University of Gaza, Gaza, Palestine, in 2011, and the M.Sc. degree in electrical engineering (industrial power) from Universiti Teknikal Malaysia, Melaka, Malaysia, in 2015. He is currently pursuing the Ph.D. degree in power systems and energy conversion with Universiti Sains Malaysia (USM), Penang, Malaysia.

JIASHEN TEH (Member, IEEE) received the B.Eng. degree (Hons.) in electrical and electronic engineering from Universiti Tenaga Nasional (UNITEN), Selangor, Malaysia, in 2010, and the Ph.D. degree in electrical and electronic engineering from the University of Manchester, Manchester, U.K., in 2016.

Since 2016, he has been a Senior Lecturer/Assistant Professor with Universiti Sains Malaysia (USM), Penang, Malaysia. In 2018, he was appointed and served as an Adjunct Professor with the Green Energy Electronic Center, National Taipei University of Technology (Taipei Tech), Taipei, Taiwan. He is currently an Adjunct Professor with the Intelligent Electric Vehicle and Green Energy Center, National Chung Hsing University (NCHU), Taichung, Taiwan. His research interests include probabilistic modeling of power systems, grid-integration of renewable energy sources, and reliability modeling of smart grid networks.

Dr. Teh is a Chartered Engineer (C.Eng.) conferred by the Engineering Council, U.K., and the Institution of Engineering and Technology (IET), a Consultant for various local companies, a member of the IEEE Power and Energy Society and the Institution of Engineers Malaysia (IEM), and a Registered Engineer in the Board of Engineers Malaysia (BEM). He received the Outstanding Publication Awards from USM, in 2017 and 2018. He is also a regular invited Reviewer of the *International Journal of Electrical Power and Energy Systems*, IEEE Access, the IEEE Transactions on Industry Applications, the IEEE Transactions on Vehicular Technology, the IEEE Transactions on Reliability, the IEEE Transactions on Industrial Electronics, and *IET Generation, Transmission and Distribution*.